Supporting Information

Highly Enantioselective "Inherently Chiral" Electroactive Materials Based on the 2,2'-Biindole Atropisomeric Scaffold

Serena Arnaboldi,[a] Tiziana Benincori, [*b] Andrea Penoni, [b] Luca Vaghi,[c] Roberto Cirilli,[d] Sergio Abbate,[e] Giovanna Longhi,[e] Giuseppe Mazzeo,[e] Sara Grecchi,[a] Monica Panigati [a,f] and Patrizia Romana Mussini[*a]

[a.] *Dipartimento di Chimica, Università degli Studi di Milano, Via Golgi, 19, 20133 Milano (Italy) E-mail: patrizia.mussini@unimi.it*
[b.] *Dipartimento di Scienza e Alta Tecnologia, Università degli Studi dell'Insubria, via Valleggio 11, 22100 Como (Italy) E-mail: tiziana.benincori@uninsubria.it*
[c.] *Dipartimento di Scienze dei Materiali, Università di Milano-Bicocca, via R. Cozzi 55, 20125 Milano (Italy)*
[d.] *Istituto Superiore di Sanità, Centro nazionale per il controllo e la valutazione dei farmaci, Viale Regina Elena 299, 00161 Roma (Italy)*
[e.] *Dipartimento di Medicina Molecolare e Traslazionale, Università degli Studi di Brescia, Viale Europa 11, 25123 Brescia (Italy)*
[f.] *Istituto per lo Studio delle Macromolecole, Consiglio Nazionale delle Ricerche (ISMAC-CNR), Via E. Bassini, 15, 20133 Milano (Italy)*

INDEX

SI.1 Experimental Procedures

SI.1.1 Synthesis

All reactions utilizing air- and moisture-sensitive reagents were performed in dried glassware under dry argon or nitrogen. Dry solvents and reagents were used as received. Macherey–Nagel Alugram® sil G/UV 254 pre-coated plates were used for TLC analysis. Column chromatography was performed on Macherey–Nagel MN Kieselgel silica gel. Melting points were determined with a Büchi B-540 instrument. ^{1}H and ^{13}C spectra were recorded with Bruker AV400 spectrometer. Chemical shifts (δ) are expressed in parts per million (ppm), and coupling constants are given in Hz. Mass analyses were performed by using a VG 7070 EQ-HF instrument.

3,3'-Bis(2,2'-bithiophen-5-yl)-1H,1'H-2,2'-biindole. 5-Iodo-2,2'-bithiophene (4.3 eq., 5.9 g, 20.3 mmol), Pd(PPh$_3$)$_4$ (0.1 eq., 544 mg, 0.47 mmol) and K$_2$CO$_3$ (5 eq., 3.2 g, 23.5 mmol) were added to a stirred solution of 2,2,2-trifluoro-N-(2-(4-[2,2,2-trifluoro-acetylamino-phenyl]-buta-1,3-diynyl)-phenyl)-acetamide (1 eq., 1.99 g, 4.7mmol) in dry and degassed MeCN (94 mL) under a nitrogen athmosphere. The reaction mixture was stirred under reflux for 24 hours. The solvent was removed under reduced pressure and the obtained residue was diluted with AcOEt; the organic phase was washed with water, dried over MgSO$_4$ and the solvent was removed under reduced pressure. The obtained residue was purified by column chromatography (n-hexane: CH$_2$Cl$_2$ = 4 : 6) to afford the desired product as a yellow/brown solid (1.28 g, 48 %);. $m.p.$: 215°C; ^{1}H NMR (400 MHz, DMSO-d_6, δ): 11.95 (s, 2H), 7.99 (d, J = 7.6 Hz, 2H), 7.48 (d, J = 8.0 Hz, 2H), 7.40 (d, J = 4.4 Hz, 2H), 7.29 (t, J = 5.2 Hz, 2H), 7.23 (t, J = 5.2 Hz, 2H), 7.12 (d, J = 3.6 Hz, 2H), 7.09 (d, J = 3.6 Hz, 2H), 7.00 (dd, J = 5.2 Hz, J = 4.0 Hz, 2H), 6.88 (d, J = 4.0 Hz, 2H); ^{13}C NMR (100 MHz, DMSO-d_6, δ): = 137.1, 136.8, 136.4, 134.3, 128.7, 126.8, 125.9, 125.3, 124.7, 124.6, 123.7, 123.4, 120.9, 120.0, 112.4, 110.9; M.S. (EI): 560 (100%).

3,3'-Bis(2,2'-bithiophen-5-yl)-1,1'-dimethyl-1H,1'H-2,2'-biindole: (N-Me-IND)$_2$-T$_4$. 3,3'-Di([2,2'-bithiophen]-5-yl)-1H,1'H-2,2'-biindole (1 eq., 310 mg, 0.55 mmol) was dissolved in dry DMF (3 mL) and the solution was cooled at 0°C. KOH (6.5 eq., 200 mg, 3.56 mmol) was added and the solution was stirred at that temperature for 10 minutes. The reaction mixture was allowed to reach room temperature and then methyl iodide (10 eq., 300 µL, 5.53 mmol) was added one pot. The reaction mixture was stirred at room temperature for 36 hours. The solvent was removed under reduced pressure and the residue was dissolved into CH$_2$Cl$_2$; the organic phase was washed with water and brine, then dried over MgSO$_4$, filtered and the solvent was removed under reduced pressure. The obtained residue was purified by column chromatography (n-hexane : CH$_2$Cl$_2$ = 8 : 2) to afford the desired product as a yellow solid (228 mg, 70 %); ^{1}H NMR (400 MHz, CDCl$_3$, δ): = 8.19 (d, J = 7.8 Hz, 2H), 7.45-7.32 (m, 6H), 7.14 (d, J = 5.1 Hz, 2H), 7.03 -7.01 (m, 4H), 6.97-6.95 (m, 2H), 6.81 (d, J = 3.9, 2H), 3.48 (s, 6H); ^{13}C NMR (CDCl$_3$, 100 MHz): δ = 137.7, 137.6, 135.8, 135.2, 127.7, 126.9, 125.7, 124.3, 124.2, 123.8, 123.4, 123.2, 120.8, 120.6, 112.9, 110.1, 30.3; M.S. (EI): 588.1 (100%).

Preparation of oligo-1.

A solution of the racemic 1 (70 mg, 0.118mmol) in dry CHCl$_3$ (10 mL) was added dropwise under a nitrogen atmosphere into a slurry of FeCl3 (90 mg, 0.55 mmol) in dry CHCl$_3$ (90 mL), under stirring, at room temperature, within 2 hours. The dark purple mixture was stirred overnight, then the volume of the solvent was reduced to 50 mL by evaporation under reduced pressure and the remaining solution was poured into MeOH (80 mL). The mixture became bright orange, and the precipitate was recovered by filtration and suspended in MeOH (30 mL), then hydrazine (4 drops) was added. The orangered solid (60 mg) was recovered by filtration and extracted with THF using a Soxhlet apparatus to remove insoluble iron-containing materials gives an orange residue that, after removal of some unreacted starting material by column chromatography,

SI.1.2 Enantioselective HPLC

HPLC enantioseparations of **1** were performed by using stainless-steel Chiralpak IB (250 mm × 4.6 mm i.d. and 250 mm × 10 mm i.d.) columns. All HPLC- and spectral-grade solvents were used without further purification. The analytical HPLC apparatus consisted of a pump equipped with a Rheodyne injector, a 20 µL sample loop, a HPLC oven, and a UV/CD detector. For semipreparative separations, a 1000 µL sample loop was used.

SI.1.3 Off-column configuration stability study

In the off-column racemization study, a solution of the longer-retained enantiomer of **(N-Me-IND)$_2$-T$_4$** (concentration about 0.1 mg mL^{-1}) in ethyl acetate was held at 60 °C in a closed vessel. The temperature was monitored by using a Julabo thermostat. Samples were withdrawn at fixed time intervals and analyzed by HPLC on the Chiralpak IB (250 mm × 4.6 mm i.d.) column under the analytical conditions reported in **Figure 3**.

SI.1.4 Chiroptical Characterization

Specific rotations of the enantiomers of **(N-Me-IND)$_2$-T$_4$**, dissolved in chloroform, were measured at the 589 nm wavelength using a Perkin Elmer polarimeter model 241 equipped with a Na lamp. The volume of the cell was 1 cm^3 and the optical path was 10 cm. The system was kept at a constant temperature of 20°C.

ECD spectra were measured with a Jasco 815SE spectrometer and 1 mm quartz cells were employed with CH$_3$CN solutions (concentration 0.0001M).

VCD spectra were taken with a Jasco FVS6000 FTIR spectrometer equipped with a VCD module, comprised of a wire-grid linear polarizer, a ZnSe Photo Elastic Modulator (PEM) to produce 50 kHz modulated circularly polarized radiation over a rather wide range (from 3000 to 800 cm^{-1}) and a liquid N$_2$-cooled MCT detector. The spectra were taken for CDCl$_3$ solution with 0.09M concentration, in a 200 μm BaF$_2$ cells. 2000 scans were collected for each spectra and subtraction of VA and VCD spectra of the solvent were performed.

CPL spectra were taken on a home-built apparatus[1], with excitation radiation brought to the sample through an optical fiber filled with water from a commercial Jasco FP8200 fluorimeter. The same solutions employed in ECD measurements were used here in 10 mm x 2 mm fluorescence quartz cells. 5 scans were accumulated for each spectrum, with 30 nm/min. scanning speed, excitation wavelength 360 nm.

SI.1.5 DFT Calculations

Prior to DFT calculations, Molecular Mechanics (MM) evaluation of stable conformers was performed. The conformers thus found were fed into the DFT module of Gaussian09[2], which was run at the B3LYP/TZVP level of theory. Calculation of Dipole and Rotational Strengths through the field-response approach[3] has been performed. VA and VCD spectra were generated by assigning 10 cm^{-1} bandwidth Lorentzian bandshape to each vibrational transition using a program resident on the Jasco VCD Software package. A scaling factor of 0.98 was applied to all bands. Time Dependent DFT calculations were also performed to predict ECD spectra[4]. The CAM-B3LYP functional was employed. Fifty transitions were considered. To plot the resulting spectra we assumed a 0.2 eV bandwidth for Gaussian type bands. Finally, DFT was used also to check interconversion mechanisms between the *P* and *M* configurations of **(N-Me-IND)$_2$-T$_4$**. After an explorative scan at PM6 level from the lowest energy conformer of Table BS1 the transition state structure has been optimized as at B3LYP/TZVP level, only one imaginary frequency has been obtained.

Comparison between neutral and charged structure have been performed considering optimization at CAM-B3LYP/TZVP level.

SI.1.6 Electrochemistry

a. Characterization and electrooligomerization of the monomer 1

Monomer **1** was characterized by cyclic voltammetry, at scan rates ranging from 0.02 to 2 V·s^{-1}, using an Autolab PGSTAT potentiostat of Eco-Chemie (Utrecht, The Netherlands), run by a PC with the GPES software. The substrate working solutions (3 cm^3) were 5·10^{-4} M in methylene dichloride (DCM, Sigma Aldrich analytical grade) or 5·10^{-4} M in acetonitrile (ACN, Sigma-Aldrich, analytical grade on molecular sieves) with 0.1 M tetrabutylammonium hexafluorophosphate, TBAPF$_6$, (Fluka, electrochemical grade) as supporting electrolyte; solutions were deaerated by N$_2$ purging before each experiment, the cell being equipped with a presaturator to grant constant working volume. The working electrode was a 0.031 cm^2 glassy carbon (GC) disk embedded in glass (*S* = 0.031 cm^2, Metrohm). The optimized finishing procedure for the disk electrode consisted in surface polishing with a diamond powder of 1 μm diameter (Aldrich) on a wet DP-Nap cloth (Struers®). The counter electrode was a platinum one. The reference electrode was an aqueous saturated calomel electrode (SCE) operating in a double bridge, filled with the working medium, to avoid water and KCl leakage into the working solution. The ohmic potential drop was compensated by the positive feedback technique.

The conducting oligomer films were electrodeposited from racemic or enantiopure monomer solutions (0.00093 M in DCM + 0.1 M TBAP, tetrabutylammonium perchlorate), by repeated oxidative potential cycling at 0.2 V s^{-1} around the monomer fourth oxidation peak, followed by repeated stability cycles in a monomer-free solution (DCM + 0.1 M TBAP).

b. Enantiorecognition Tests

The enantiorecognition tests were carried out in a minicell with GC embedded in glass (*S* = 0.031 cm^2) as working electrode covered with the enantiopure films oligo-**(S)-(N-Me-IND)$_2$T$_4$** and oligo-**(R)-(N-Me-IND)$_2$T$_4$** (prepared according the above protocol), a Pt disk as a counter electrode and an aqueous saturated calomel as a reference electrode always inserted into a glass jacket filled with the same cell background solution.

Chiral electrode surfaces were immersed in solutions containing the enantiomers of the chiral probes; CVs were recorded at 0.05 V s^{-1} potential scan rate for each probe + selector combinations.

The analyzed chiral probes were: *i)* (*S*)- and (*R*)-N,N-dimethyl-1-ferrocenylethylamine probes (2·10^{-3} M, Sigma-Aldrich, ≥ 97%) dissolved in DCM + TBAP 0.1 M, *ii)* 1.9 mg of Madopar® (Roche) containing 100 mg + 25

mg of 3,4-dihydroxy-L-phenylalanine (L-DOPA) and benserazide, respectively, dissolved in water (for trace analysis, Sigma-Aldrich) with 0.05 M of hydrochloric acid ($\geq$ 37%, for trace analysis Sigma-Aldrich), *iii*) (*S*)-(+)-ketoprofen ($2 \cdot 10^{-3}$ M, Sigma-Aldrich, 99%) in dichloromethane with TBAP 0.1 M as supporting electrolyte.

For sake of comparison CVs of L-DOPA (~1.5 mg) and beserazide (~0.4 mg), dissolved in water with 0.05 M of hydrochloric acid, were recorded separately on bare GC electrode at 0.5 V s^{-1} potential scan rate.

c. Magnetoelectrochemistry

Magnetoelectrochemistry experiments were carried out by using as working electrode an ITO slice (0.8 $\times$ 4.5 cm^2) coated glass where the enantiopure (*R*)- and (*S*)-oligo-**1** films were electrodeposited according to the procedure described in the previous paragraph. The magnetic field was applied by an external magnet (nickel coated NdFeB B88X0 Grade N42 K&J Magnet, Inc.; magnetic field strength at the surface = 6353 Gauss) placed at a distance of ca. 2 mm from the film|ITO interface.

Cyclicvoltammograms of the achiral redox couple $Fe(CN)_6^{3-}$| $Fe(CN)_6^{4-}$ (with each component at 2.5 mM concentration and 400 mM KCl as supporting electrolyte) were recorded at 0.05 V s^{-1} potential scan rate in a cuvette by flipping the external magnet north *vs* south orientations.

SI.2 Detailed account of ab initio calculations and evaluation of racemization barriers of the starting monomer

A thorough conformational analysis of **(N-Me-IND)$_2$-T$_4$** has been conducted, since many conformers are possible due to the mobility of the thiophene pendant groups (**Table SI.2**).

Conformer	ΔG	θ1	θ2	φ1	φ2	δ
1t	0.00	158.2	158.2	143.7	143.7	115.5
2t	0.51	-158.2	-158.2	-37.6	-37.6	115.5
3t	0.77	-157.4	155.8	136.6	32.5	95.3
4t	0.90	-156.5	-156.9	-150.4	-35.3	99.4
5t	0.93	154.8	154.8	38.5	38.5	79.2
6t	1.02	-157.7	157.0	-35.8	-151.2	99.8
7t	1.08	154.2	-155.1	36.8	-143.6	80.4
8t	1.45	154.3	-156.1	32.1	-37.3	98.0
1c	0.78	-157.7	32.2	143.5	144.3	114.9
2c	1.17	-33.7	-157.2	-148.5	137.3	95.9
3c	1.26	155.0	-33.3	37.8	37.1	80.2
4c	1.27	-33.1	-158.2	142.6	-36.9	115.8
5c	1.28	-158.2	32.9	-38.0	-38.1	116.0
6c	1.34	-157.3	33.3	137.3	-148.9	96.2
7c	1.35	-157.3	-32.9	141.9	-35.8	115.9
8c	1.44	157.6	33.2	-147.6	135.9	95.6
9c	1.49	-156.9	-33.1	136.1	33.1	94.9
10c	1.53	-156.9	34.0	136.5	32.7	95.0
11c	1.55	-32.4	-157.6	-37.0	-37.4	115.5

All S-S trans

↓

S-S cis + trans

↓

Table SI.2 DFT relative Gibbs free energy (kcal/mol) and values (degrees) for the most important dihedral angles characterizing the conformers of the (*S*) enantiomer of **(N-Me-IND)$_2$-T$_4$**. For the definition of dihedral angles see scheme on the lower side.

Figure SI.2.1 provides the comparison of the most stable conformer of **BT$_2$-T$_4$** with the two lowest energy conformers of **(N-Me-IND)$_2$-T$_4$**, each one with C_2-symmetry.

BT$_2$-T$_4$

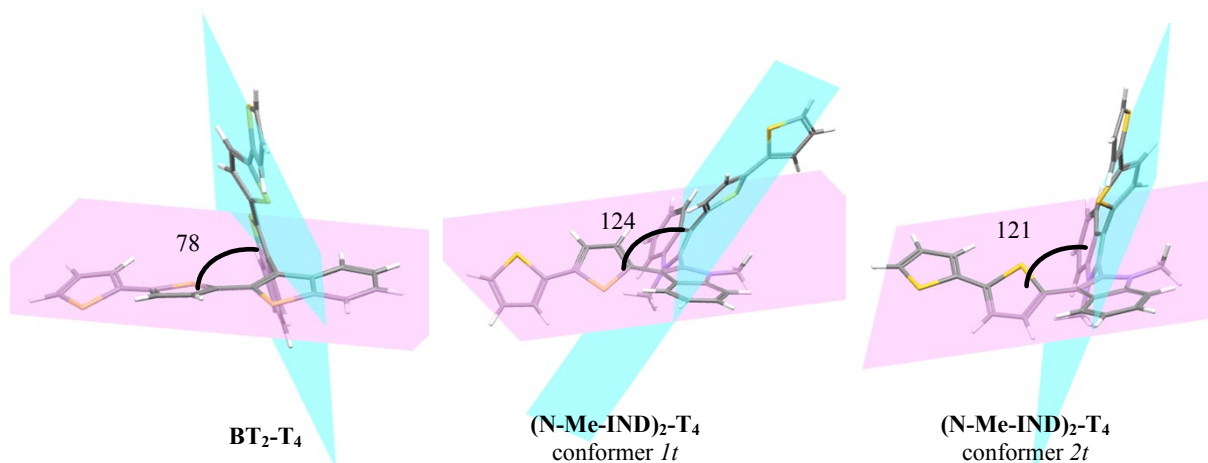**(N-Me-IND)$_2$-T$_4$** conformer *1t*

(N-Me-IND)$_2$-T$_4$ conformer *2t*

Figure SI.2.1: Structure of the most stable conformers of **BT$_2$-T$_4$** (left) and of the two lowest energy conformers of **(N-Me-IND)$_2$-T$_4$** (middle, right). DFT calculations at B3LYP/TZVP level of theory. Interplanar dihedral angles given in the three figures. (Planes fitting the nine atoms of each core moiety highlight mutual orientations.).

The orientation of the thiophene rings in **BT$_2$-T$_4$** is a consequence of the favoured *trans* disposition of S atoms, which are also present in the bithianaphtene moiety. The most stable **(N-Me-IND)$_2$-T$_4$** conformer, *1t*, features an opposite orientation of the thiophene rings, while conformer *2t*, similar to the **BT$_2$-T$_4$** major one, is less populated. In the case of **(N-Me-IND)$_2$-T$_4$** all thiophene rings are tilted by a noticeable amount with respect to the drawn planes.

To gain insight into the oxidation/reduction process, the two most populated conformers have been also optimized in their charged states (cation and dication as well as anion and dianion). Changes in the angle between the two **N-Me-IND-T$_2$** moieties upon charge state variation are not very pronounced, as exemplified by their superimposition (**Figure SI.2.2**).

Figure SI.2.2. Superposition of the structures calculated at CAM-B3LYP/TZVP level for **(N-Me-IND)$_2$-T$_4$** in its neutral state and four charged ones (cation and dication as well as anion and dianion).

Upon charging, the thiophene chains flatten and the structure evolves from aromatic to quinoid (with the core assuming an indigoid structure), as expected;[5-7] the more quinoid is the structure, the flatter are the thiophene chains, as observed in similar systems.[7]

In order to evidence where the defect, upon oxidation/reduction is localized within the molecule, **Figure SI.2.3** provides calculated lengths for the CC bonds marked in bold in the formulas, as a function of the charge state.
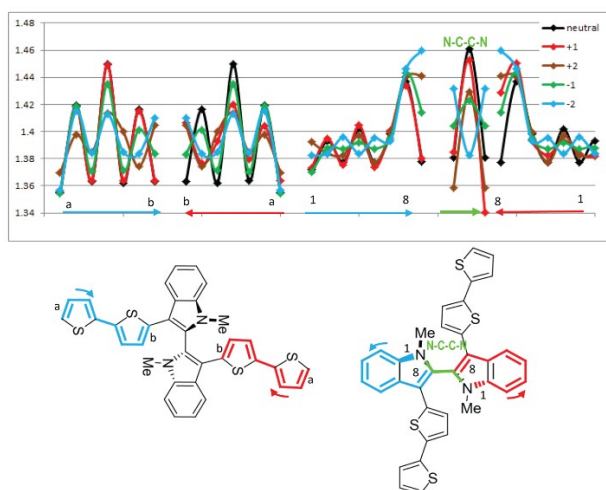

Figure SI.2.3. CC bond lengths (Å) of **(N-Me-IND)$_2$-T$_4$**, calculated on the optimized structure of the most populated conformer in its neutral and charged states.

The results support the formerly discussed progressive involvement of the two pyrrole-thiophene symmetrical systems in the first and second oxidation processes as equivalent, reciprocally interacting redox centers. In particular:

- the cation appears to be mainly perturbed on the pyrrole unit of one moiety of the indole core, also involving the adjacent thiophene ring, leaving the other core moiety nearly unchanged;
- the dication symmetrically involves the pyrrole units of both core moieties together with their adjacent thiophene rings;
- in both cases, the external thiophene rings are only slightly perturbed, which justifies the experimental observation of no radical coupling activation before the third oxidation peak.
- the anion and dianion species involve the pyrrole-bithiophene system, with a remarkable inversion of a central double/single bond sequence particularly in the symmetrical dianion, implying the above mentioned quinoid structure with an indigo-like core.

Since the molecule is chiral, we can gain information about the interconversion between the two enantiomers optimizing the racemization transition state (TS). The energy difference between TS and the lowest energy conformer is rather low, *i.e.* about 27 Kcal/mol; however it is enough to guarantee the stability of enantiomers at room temperature. TS corresponds to a geometry with inversion symmetry and with the two indole moieties in the same plane (**Figure SI.2.4**).
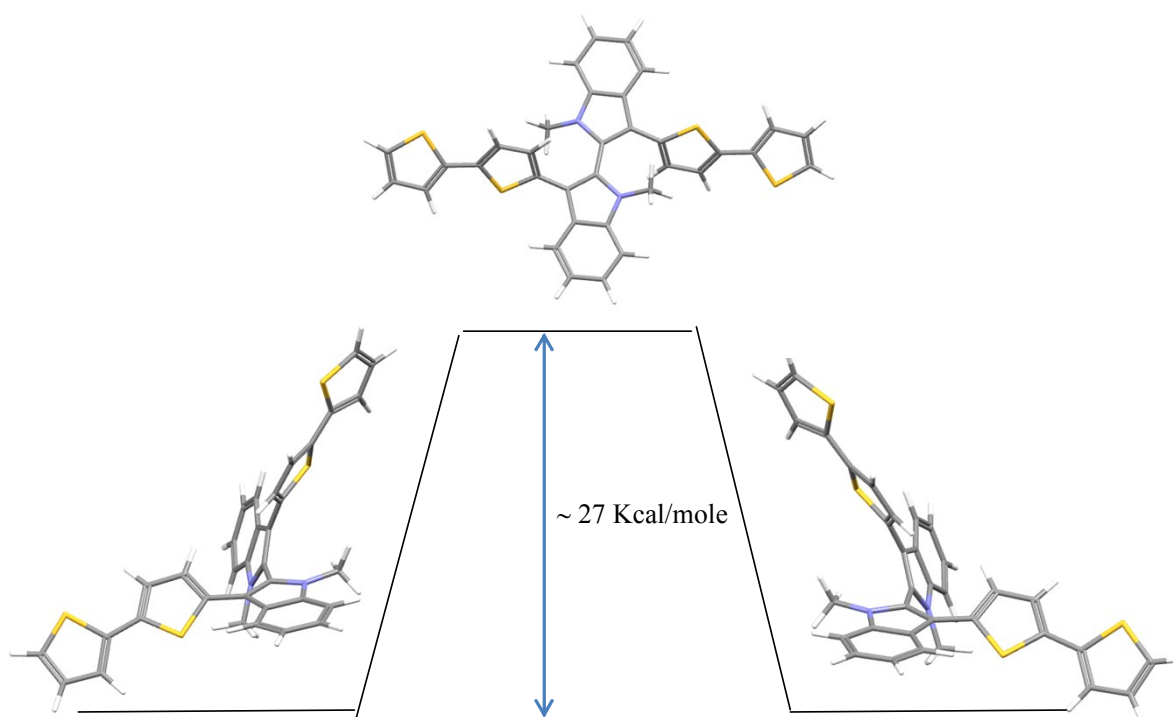

~ 27 Kcal/mole

Figure SI.2.4. Lowest energy structures of the two enantiomers of **(N-Me-IND)₂-T₄** and of their interconvertion transition state structure, as obtained by B3LYP/TZVP calculations.
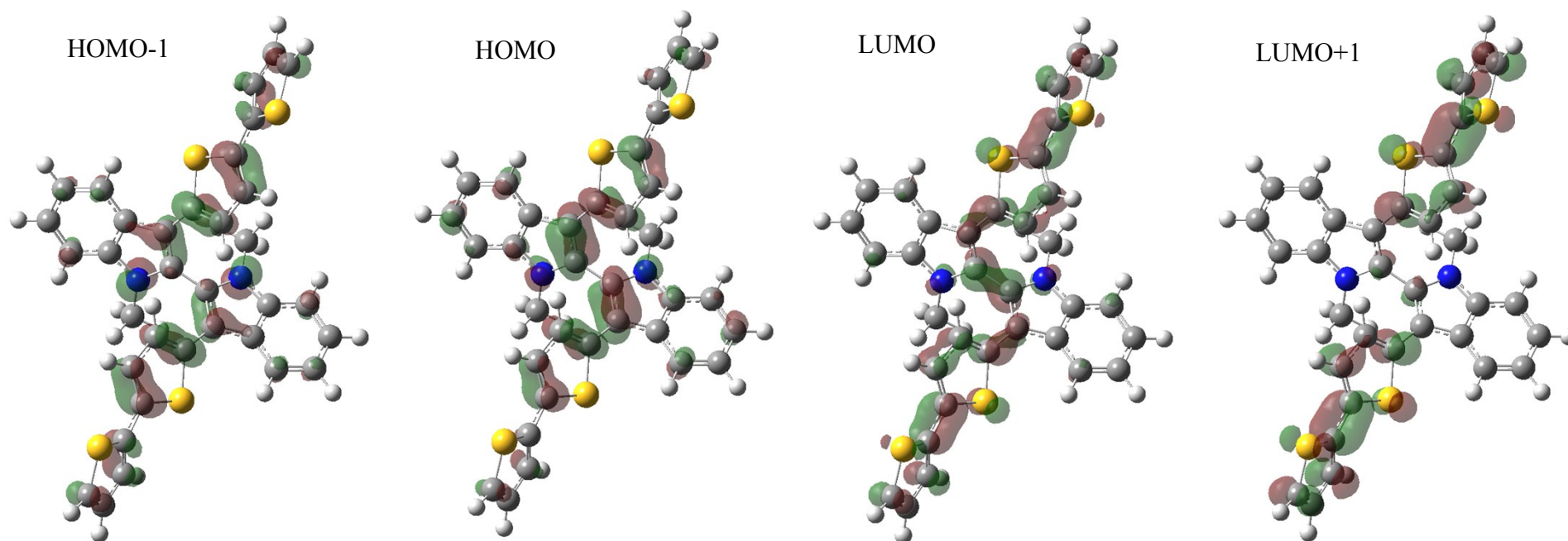
HOMO-1   HOMO   LUMO   LUMO+1

Figure SI.2.5. Isovalue surfaces for HOMO-1, HOMO, LUMO and LUMO+1 orbitals involved in the CD exciton couplet, for the lowest energy conformer. First excitation: HOMO→LUMO (0.66), HOMO-1→LUMO +1 (-0.28); second excitation: HOMO-1→LUMO (0.48), HOMO→LUMO+1 (-0.47).
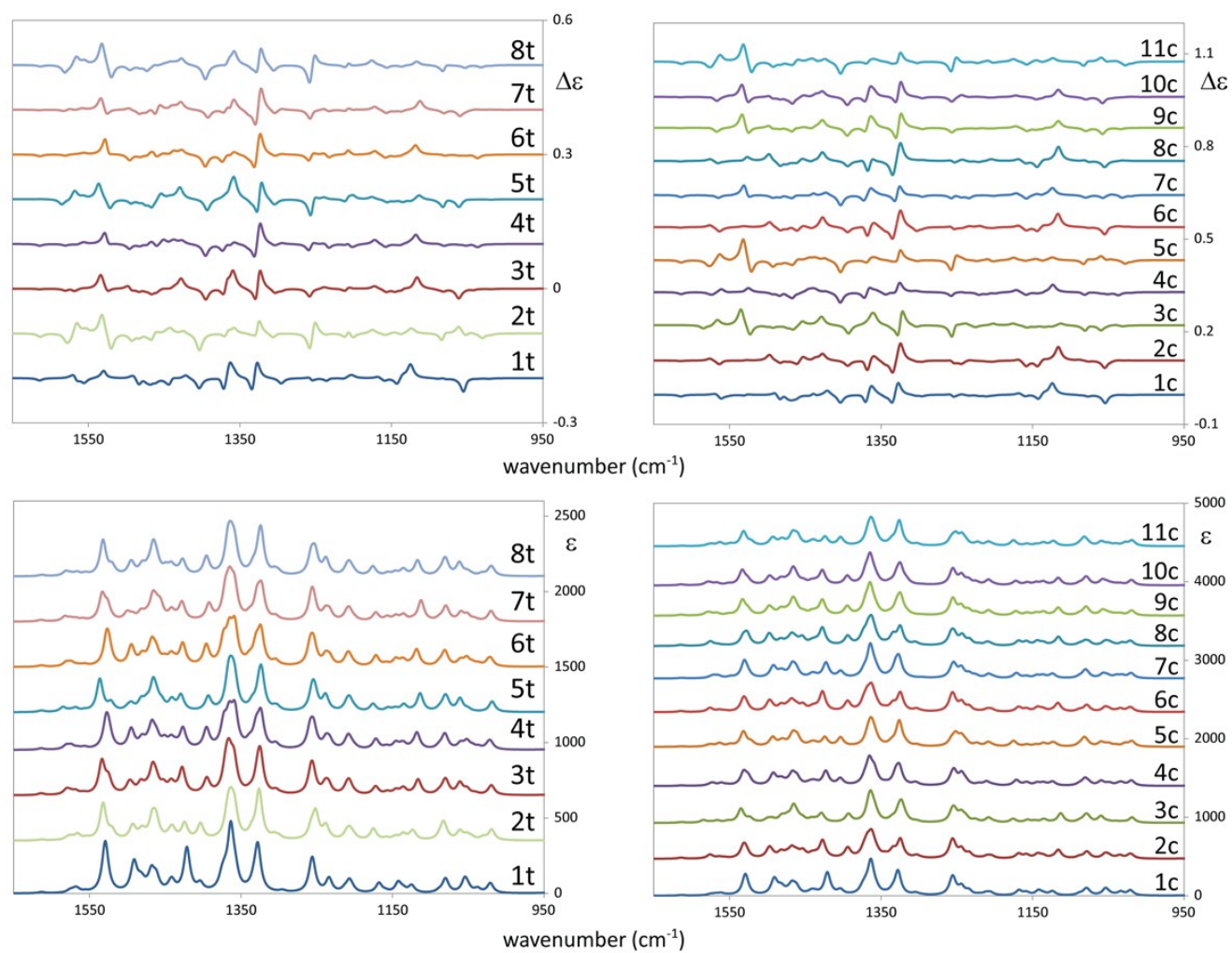
Figure SI.2.6 Calculated VCD and IR spectra of all conformers of **Table 1** for the (*S*) enantiomer of **(N-Me-IND)₂-T₄**. Wavenumbers have been scaled by 0.98.
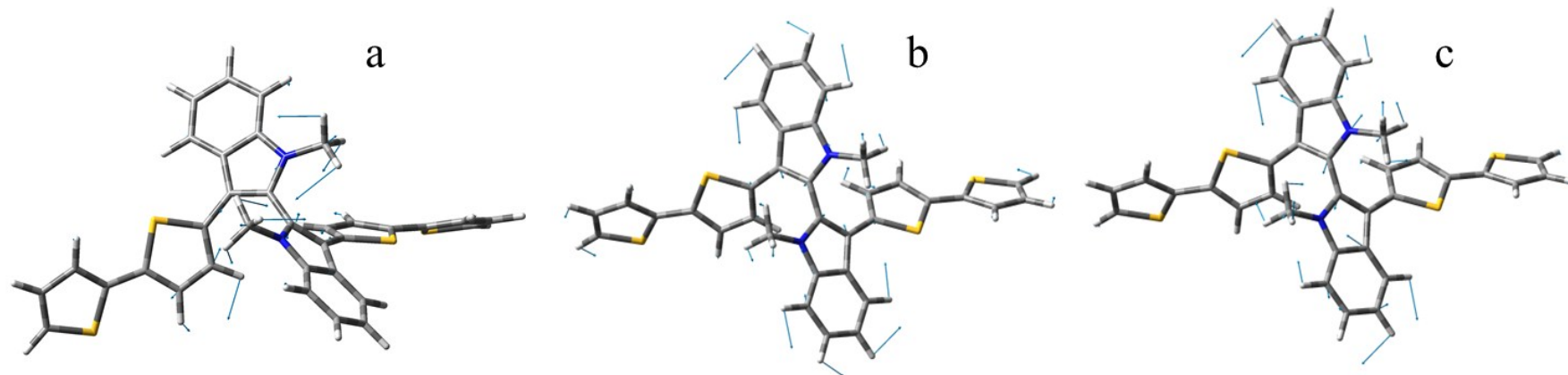
Figure SI.2.7 Normal modes, mostly localized on the N- methyl-biindole moiety, presenting a common VCD pattern throughout the various conformers: **a)** negative feature at about 1400 cm^{-1}, scaled wavenumber; **b,c)** doublet centered at about 1320 cm^{-1}, scaled wavenumber.

SI.3 Chiral HPLC off-column configuration stability studies

The configurational stability of **1** was established by classical batch-wise kinetic measurements (<u>see section SI.1.3. for details</u>). These studies highlighted a high stability against racemization at room temperature, the racemization energy barrier at 60°C being 29.9 kcal mol^{-1} in ethyl acetate solution. (**Figure 3**)

SI.4 Detailed account of the electrochemical investigation of the monomer properties

The electronic properties of the monomer were investigated from the electrochemical point of view, by cyclic voltammetry. A selection of results is reported in **Figure 2a, b** (a magnification is reported below in **Figure SI.4.1**) and **Table 1**.
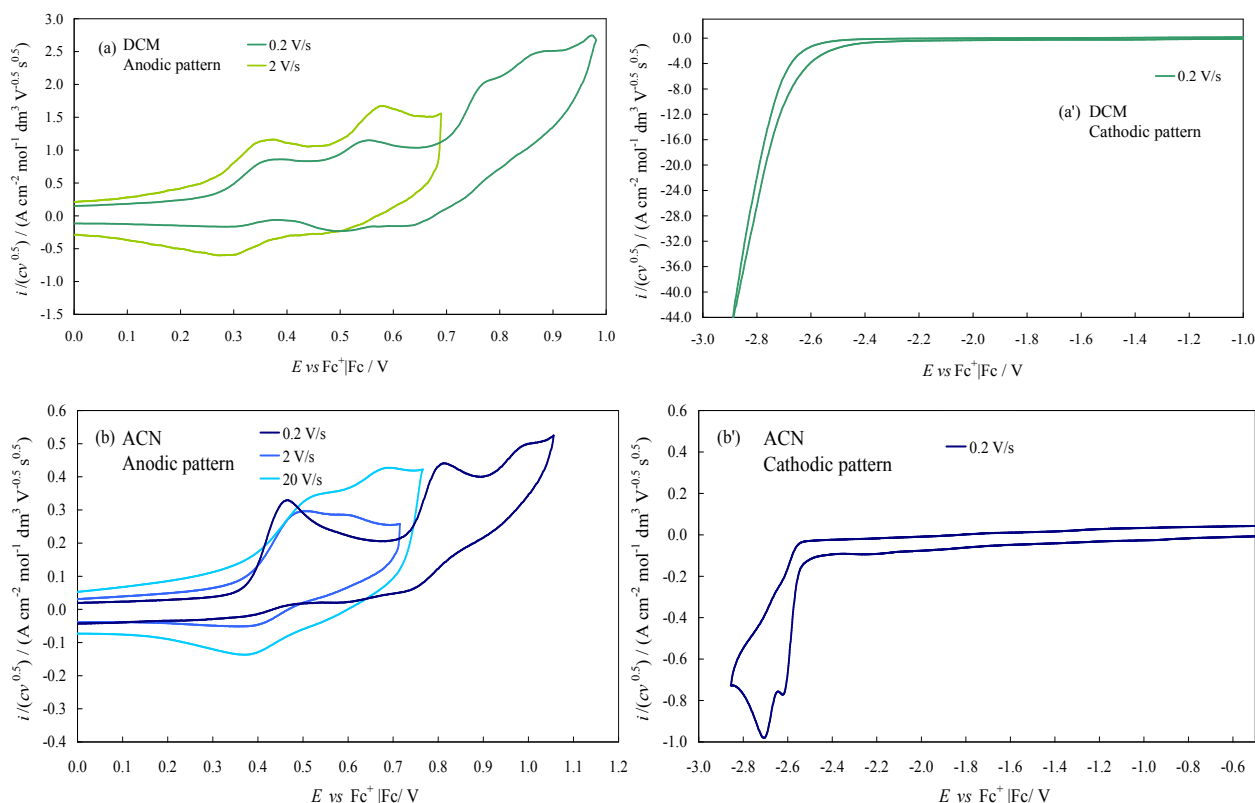

Figure SI.4.1. Extension of CV patterns of monomer **1** in (a), (a') anodic and cathodic pattern, respectively in DCM; (b), (b') anodic and cathodic pattern, respectively in ACN, with 0.1 M TBAPF$_6$ supporting electrolyte, on GC electrode.

The oxidative region of the CV pattern recorded in dichloromethane (**Figure 2a**) features
• a first system of twin monoelectronic peaks, the first one electrochemically reversible (peak potentials nearly constant with scan rate→ facile electron transfer) and chemically reversible (symmetrical return peak → stable electron transfer product), the second one approaching full reversibility with increasing scan rate.
• a second system of two nearly merging irreversible peaks, very similar to the one observed for **BT$_2$-T$_4$** in DCM solvent.[8]
The first system, which is located at peak potentials significantly less positive than the **BT$_2$-T$_4$** case, should account for two oxidation processes involving two equivalent redox sites, electron richer than in the **BT$_2$-T$_4$** case, and partially interacting as evidenced by the significant peak potential splitting.
As discussed later, each redox site could be mainly localized on the pyrrole ring of a core moiety, with nearly no involvement of the condensed benzene ring but with partial involvement of the conjugated bithiophene chain, particularly the adjacent thiophene ring while the terminal one is nearly unperturbed. Since pyrrole is electron richer than thiophene, (a) on one hand the pyrrole-bithiophene system is electron richer than terthiophene, justifying the less positive oxidation potentials with respect to **BT$_2$-T$_4$**; (b) on the other hand the charge density.
is in this case mainly concentrated close to the pyrrolic unit, that is, close to the monomer core; this can justify the chemical stability of both radical cation and dication, as confirmed both by the neat CV return peaks and by the absence of oligomer film formation upon potential cycling around the first twin peak oxidation system (see later on).
The thiophene terminals should instead be significantly involved in the second oxidative system following the first twin peak one, consistently with the peak irreversibility and the oligomerization obtained by including this second peak system in the potential cycles.
Unfortunately, the narrow DCM potential window on the reduction side prevents observation of the reduction peaks of monomer **1**, however, they are clearly visible in acetonitrile (**Figure 2b**). In particular, they

13

are located at potentials significantly more negative than in the **BT₂-T₄** case. DFT calculations indicate a LUMO orbital delocalized on the the pyrrole-bithiophene twin systems. The above considerations about the pyrrole electron richness both justify the negative shift of the first reduction potential and explain why upon reduction the charge density is more localized on the thiophene wings. A further intriguing clue from the theoretical computations concerns a possible quinoid structure of the dianion species, with the central bond length gradually decreasing from that typical of a single bond to that of a double bond with increasing negative charge and concurrent increase of the adjacent bond lengths from double to single (**Figure SI. 1.3**).

Interestingly, in acetonitrile the core oxidation results in a single, irreversible bielectronic peak at 0.2 V/s scan rate, implying the simultaneous involvement of both core moieties in a chemically irreversible process triggered by the first electron transfer. However, with increasing scan rate such signal evolves into a system of twin reversible peaks, with a smaller peak potential difference with respect to the DCM case at equal potential scan rate; this is consistent with the more polar ACN solvent having a more powerful screening effect than DCM on the reciprocal interactions between the equivalent indole-thiophene redox sites.

SI.5 Detailed account of the photophysical investigation

Also the photophysical properties of the monomer **(N-Me-IND)$_2$-T$_4$** (**1**), listed in **Table 1**, are studied in comparison with the ones previously reported for the analogous **BT$_2$-T$_4$** under diluted conditions (1×10^{-5} M), in air-equilibrated solution at room temperature. The absorption spectrum of **1**, recorded in DCM, displays a broad absorption band with a maximum at 364 nm, 8 nm blue-shifted with respect to that observed for **BT$_2$-T$_4$** in the same conditions, and that can be confidently attributed to a ^{1}ICT (intra-molecular charge transfer) transition from the π system of the pyrrole ring of the core (only partially extended on the π system of the thiophene chain, see DFT calculations) to the π^* of the bi-thiophene wing.

The change of the nature of the excited state with respect to **BT$_2$-T$_4$** is due to the presence of the pyrrole ring which has a double effect on the electronic levels of **1**. Actually, the electron-richer pyrrole ring, more easily oxidable (as discussed in the Electrochemical Section **SI.4**), affords both an increase of the HOMO level and, at the same time, a destabilization of the LUMO and LUMO+1, mainly localized on the bithiophene wings. The overall effect is a blue-shift of the absorption maximum of **1** with respect to that observed for **BT$_2$-T$_4$**. The charge transfer character of the electronic transition is further supported by the typical solvent dependence of the charge-transfer absorption band.[9] Indeed, a blue shift is observed for **1** upon increasing solvent polarity (from 367 nm in toluene to 358 nm in ACN) for **1**. It is important to note that no effect is observed on the absorption maximum of **BT$_2$-T$_4$** upon changing the solvent polarity, in agreement with the $\pi-\pi^*$ character of the electronic transition, located on the α-terthiophene chain.[10] (see **Table 1**).

Upon optical excitation in the range of 400–430 nm, monomer **1** shows intense and unstructured emission in the green region of the visible spectrum, which is independent of the excitation wavelength and is attributed to the radiative decay of the ICT excited state. The unstructured emission is in agreement with the lower degree of conjugation between the core and the side wings, which hampers the formation of the planar quinoid-like structure usually proposed for the excited states of oligothiophenes. Also the emission maximum is solvent-dependent (from 500 nm in toluene to 523 nm in ACN for **1**), confirming the charge transfer character of the excited state. The red shift of the emission band, observed in the more-polar solvent (opposite to that observed in absorption) is accompanied by a strong decrease of the intensity (**Table 1**), in agreement with the energy gap law (EGL).[11] As already observed in absorption, no effect is observed on the emission behaviour of **BT$_2$-T$_4$**: both the energy and the intensity of the emission spectra are the same in all the investigated solvents.
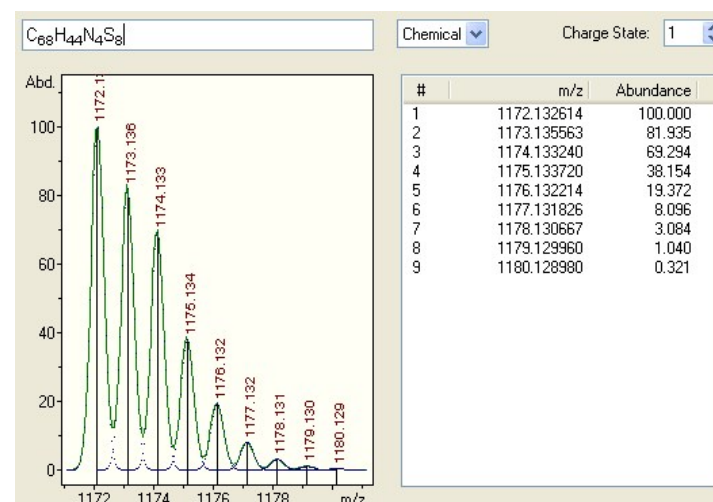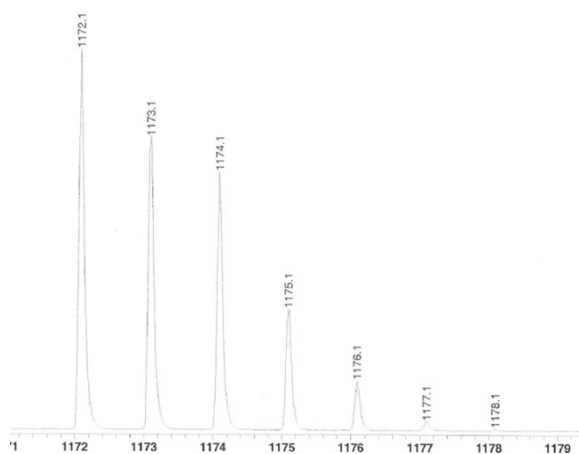
SI.6 Identification of other examples of parallel spectroscopic (Davydov) splitting and CV peak splitting in other atropoisomeric inherently chiral systems

Careful reexamination of former works confirms the presence of both spectroscopic and CV peak splitting in other atropoisomeric inherently chiral systems with two equivalent redox sites/chro-mophore moieties:

- **BT_2T_4** (bibenzothiophene-based atropisomeric monomer): monomer CV peak splitting in CH_2Cl_2 reported in [8] and in the supporting information of [12]; spectroscopic (Davydov) splitting in CH_2Cl_2 evidenced as CD couplet centered on absorption maximum reported in [7].
- **BT_2CPDT_2** (bibenzothiophene-based atropisomeric monomer, with more planar wings than **BT_2T_4** including cyclopentadithienyl units instead of bithiophene ones): monomer CV peak splitting reported in [8] (in ACN; hovewer in the less polar CH_2Cl_2 should be much larger on account of the higher reciprocal interaction between the two equivalent redox sites, as in many cases observed in our lab (unpublished data); spectroscopic (Davydov) splitting in CH_2Cl_2 evidenced as CD couplet centered on absorption maximum also reported in [8].
- **BT_2DTP_2** pyrrole (another bibenzothiophene-based atropisomeric monomer, with more planar wings than **BT_2T_4** including dithienopyrrole units instead of bithiophene ones): monomer CV peak splitting reported in [8] (in ACN; in the less polar CH_2Cl_2 should be much larger, see above); spectroscopic (Davydov) splitting in CH_2Cl_2 evidenced as CD couplet centered on absorption maximum also reported in [8].

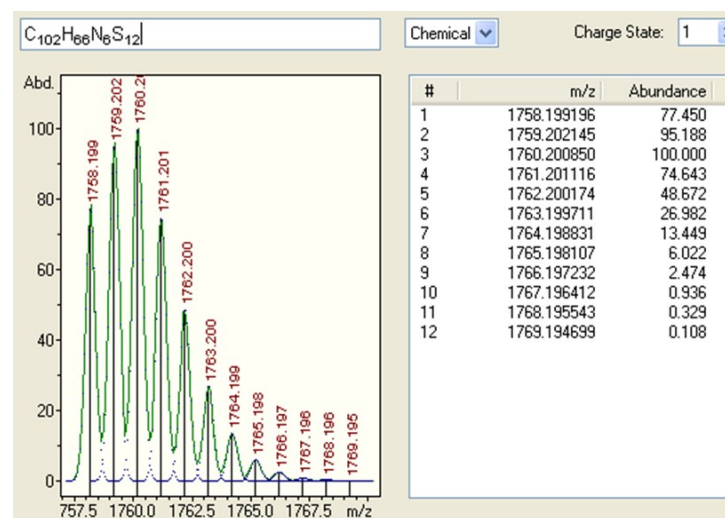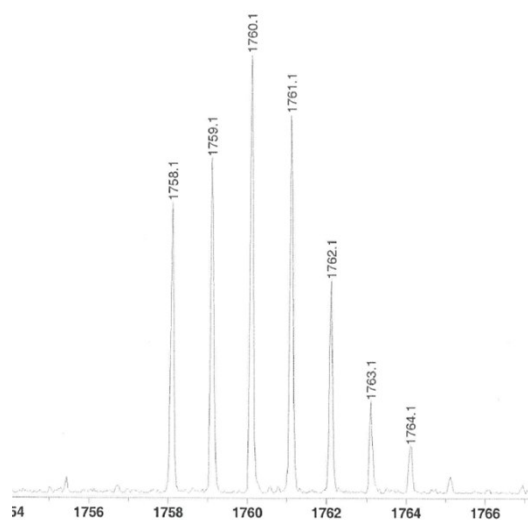## SI.7 LDI and HPLC features of oligomers

Figure SI.7.1. a) LDI experimental and calculated (right) isotopic distribution for the cyclic dimer of (**N-Me-IND**)₂-**T₄**; b) LDI experimental and calculated (right) isotopic distribution for the cyclic trimer of (**N-Me-IND**)₂-**T₄**
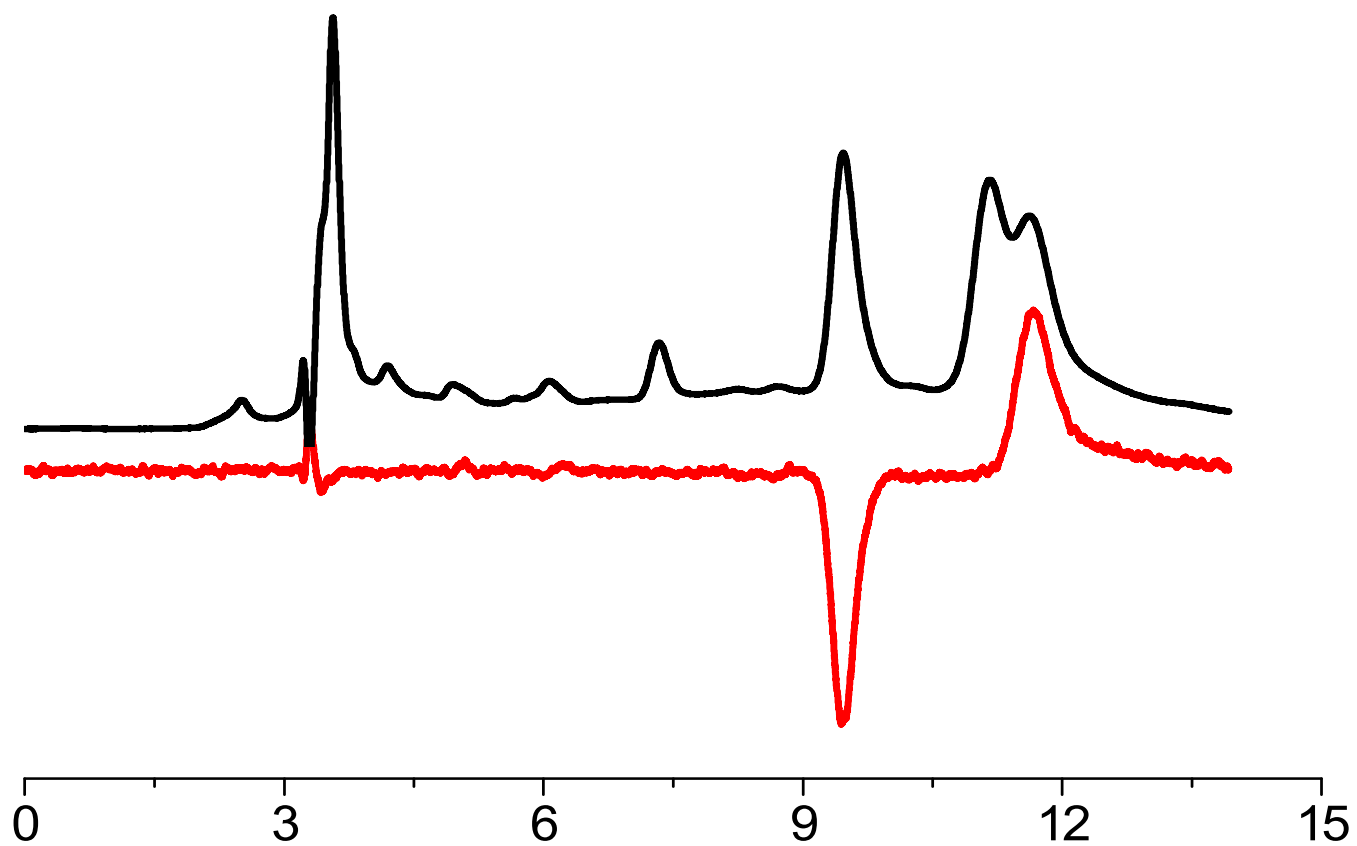
Figure SI.7.2. HPLC chromatogram of racemic cyclic dimer of (**N-Me-IND**)$_2$-**T**$_4$: CSP: Chiralpak IA (250 mm x 4.6 mm I.D); eluent: acetone-methanol 50:50; Flow rate: 1 ml/min; T = 5 °C; detector: UV (black) and CD (red) at 410 nm.
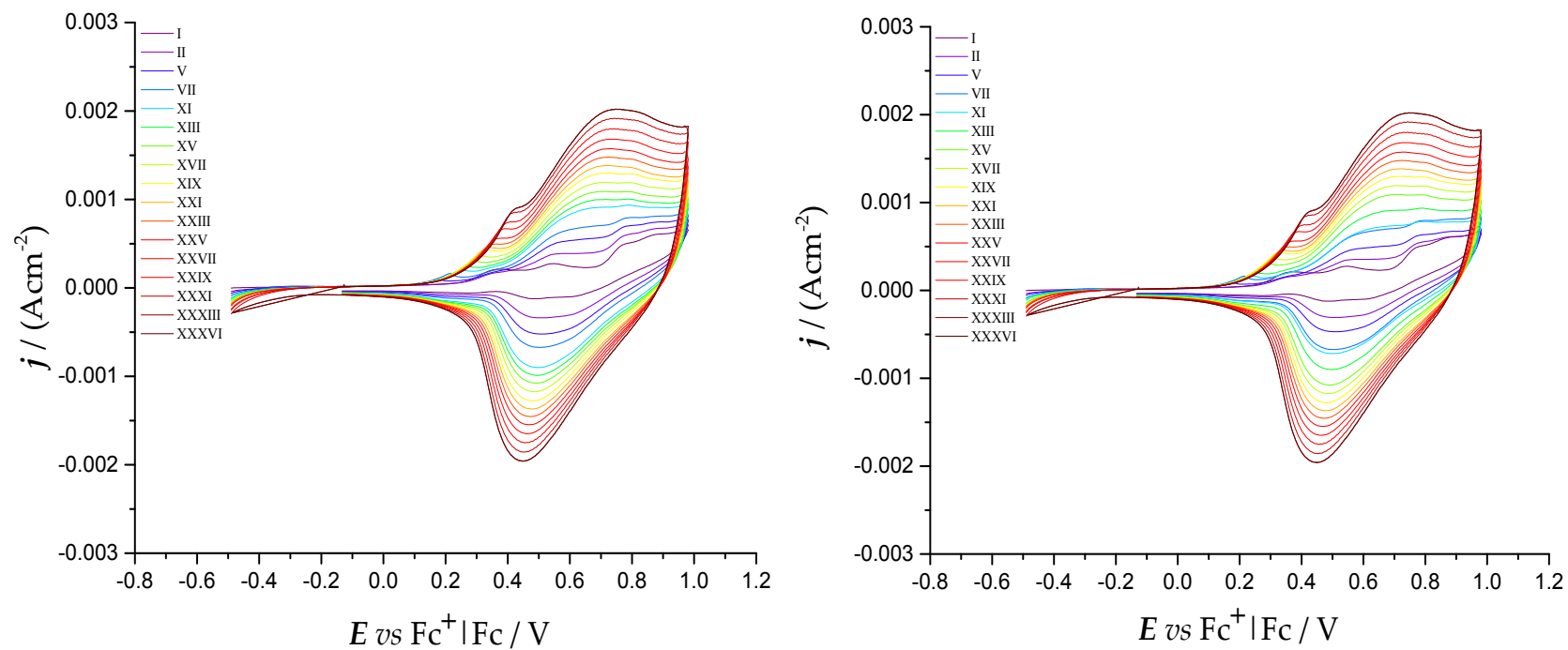
Figure SI.8.1 Electrooligomerization of enantiopure **(S)-(N-Me-IND)₂-T₄** (left) and **(R)-(N-Me-IND)₂-T₄** (right), 0.00093 M, in DCM + 0.1 M TBAP) on GC electrode at 0.2 V/s potential scan rate.

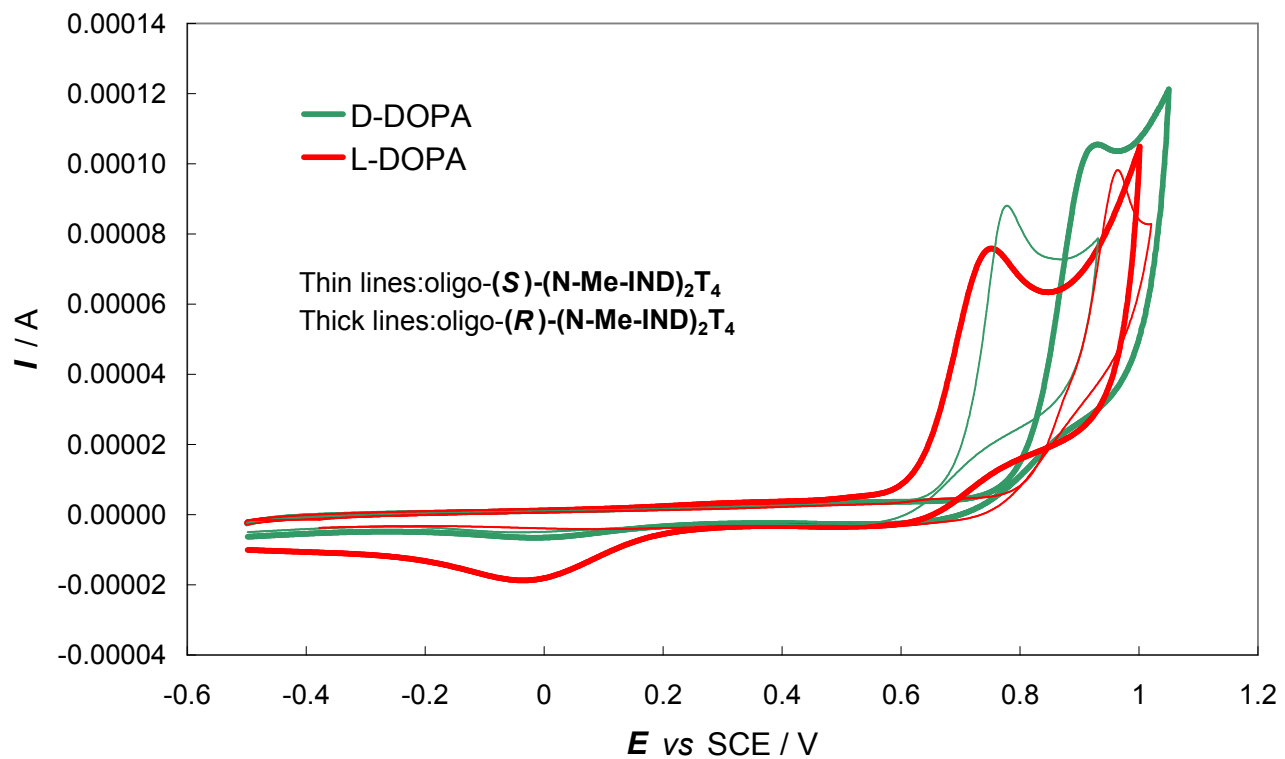## SI.9 Enantioselection tests towards L- and D- DOPA probe enantiomers

Figure SI.9 Enantioselection tests on (*R*)- and (*S*)-oligo-**1** towards DOPA antipodes. CVs were recorded at 0.05 Vs^{-1} on GC electrode in aqueous solution (HCl 0.05M).
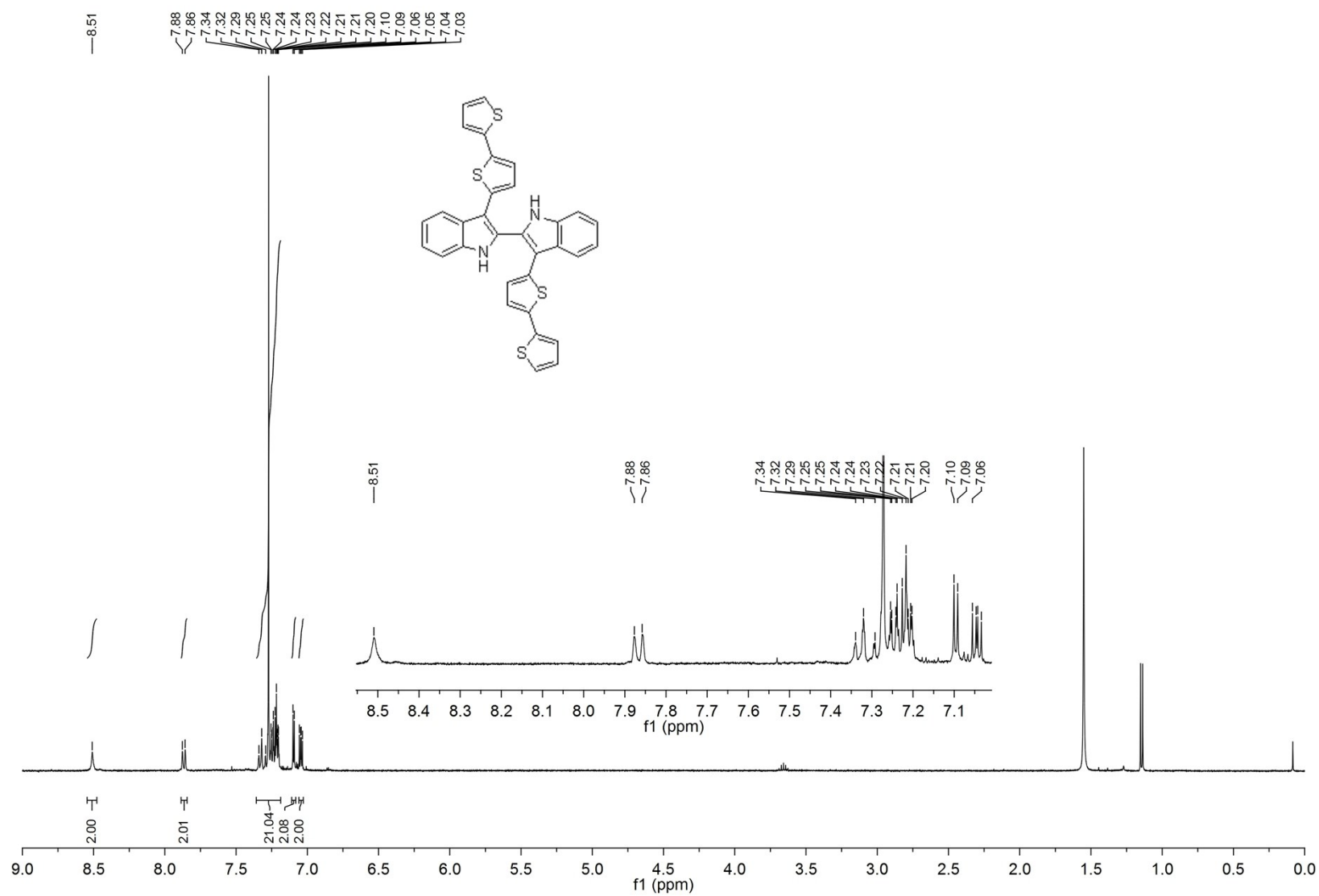
Figure SI.10.1. ¹H NMR (400 MHz, CDCl₃) of 3,3'-bis(2,2'-bithiophen-5-yl)-1*H*,1'*H*-2,2'-biindole.
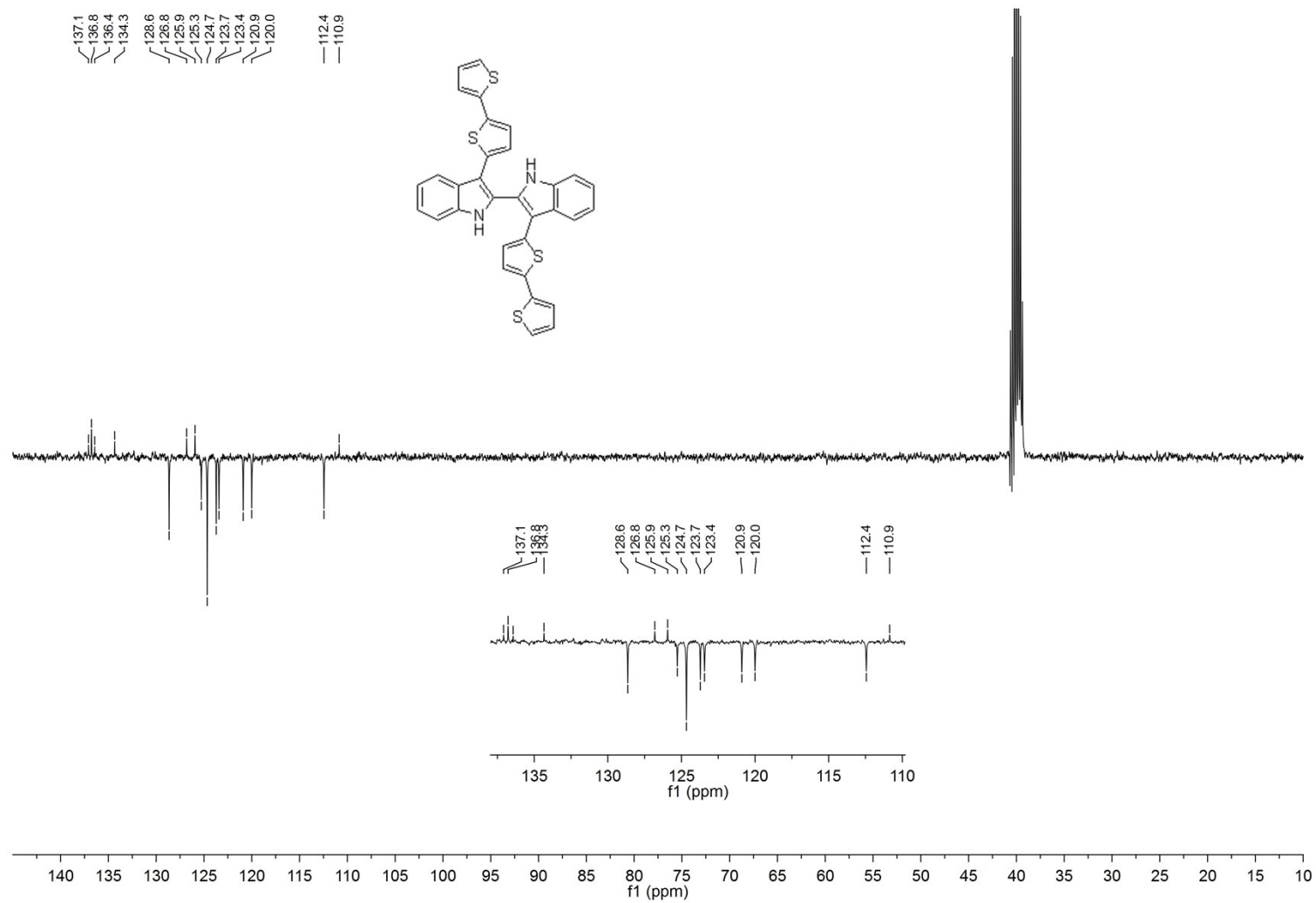
Figure SI.10.2. ^{13}C NMR (101 MHz, DMSO-d$_6$) of 3,3'-bis(2,2'-bithiophen-5-yl)-1*H*,1'*H*-2,2'-biindole.
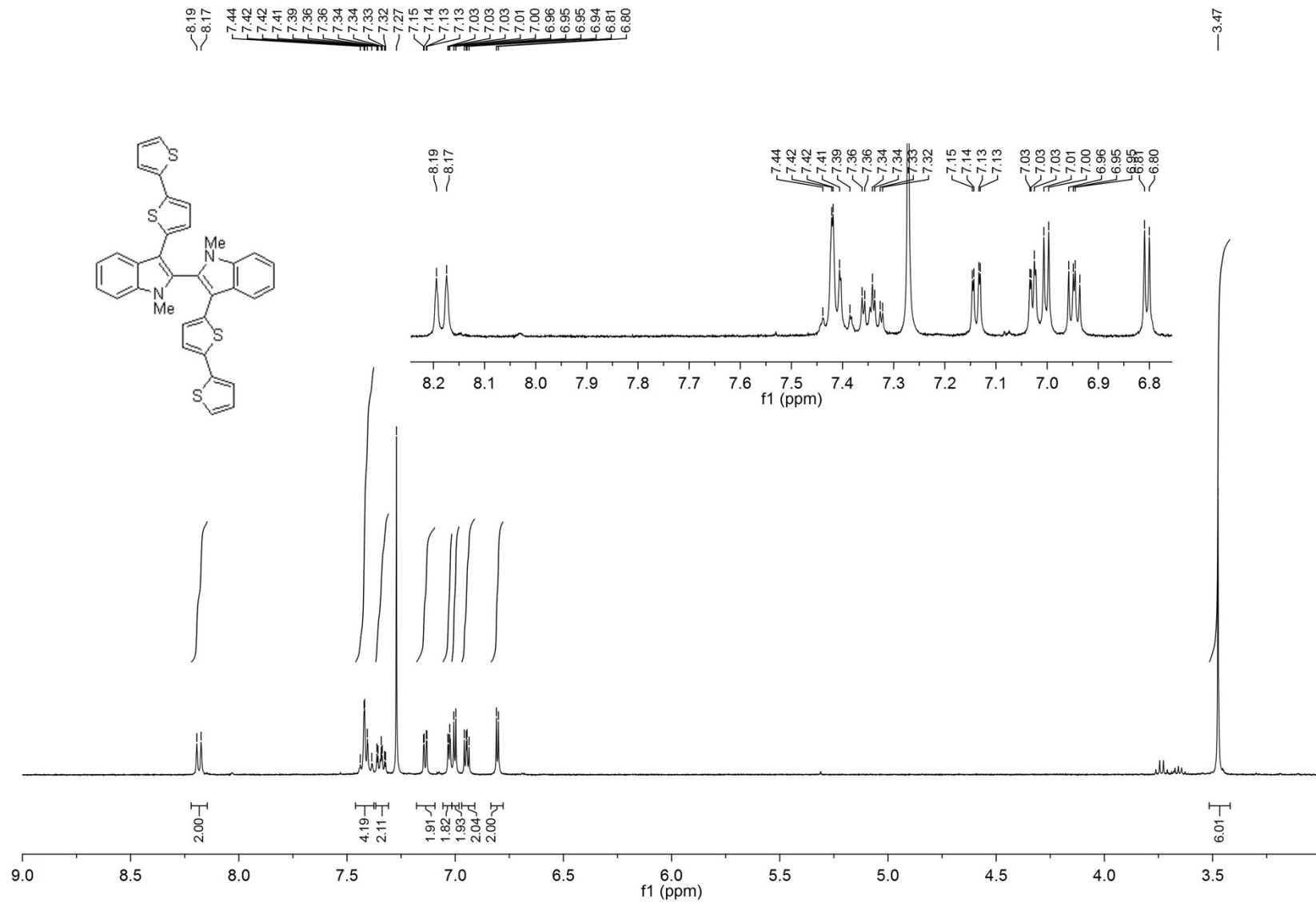
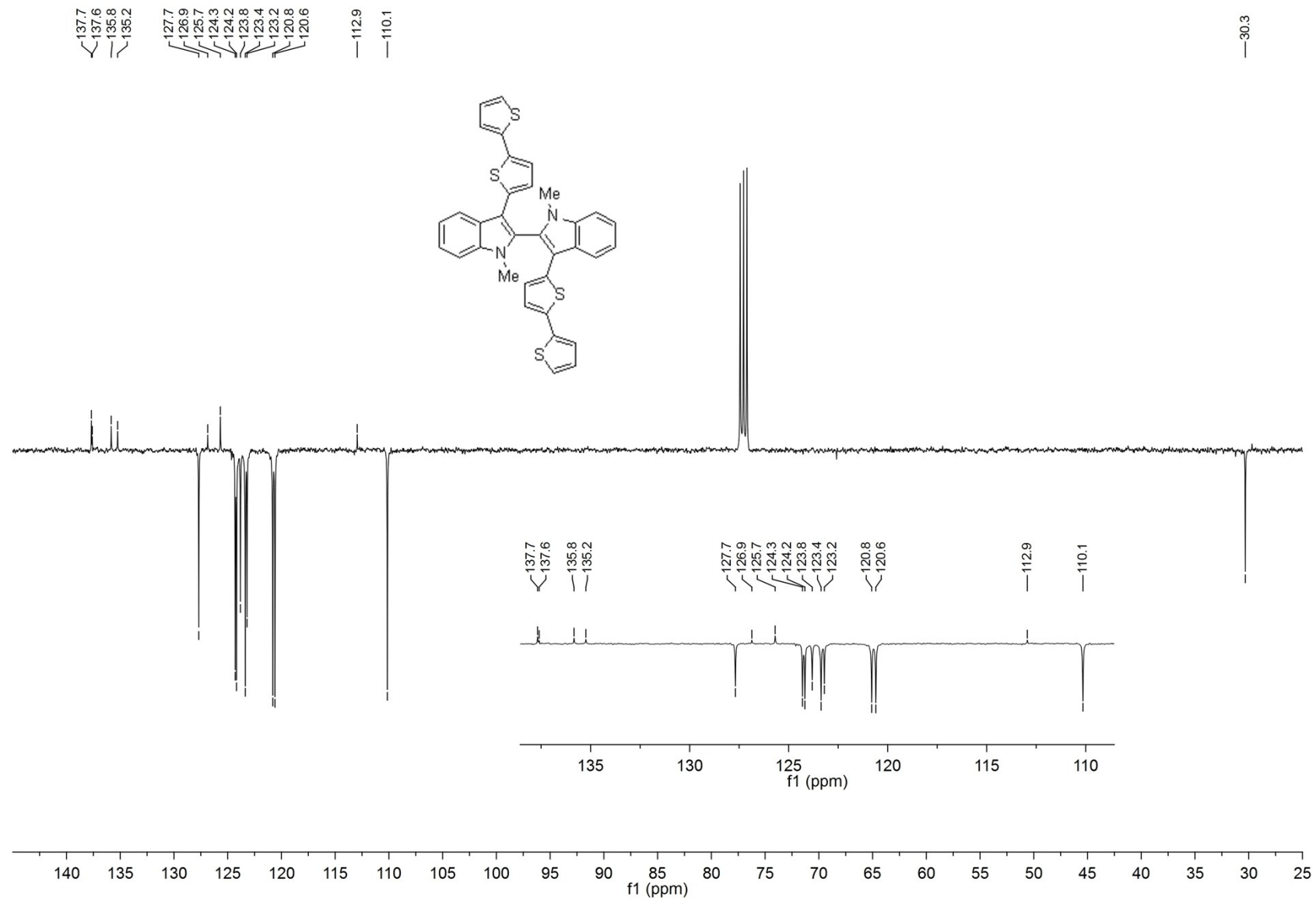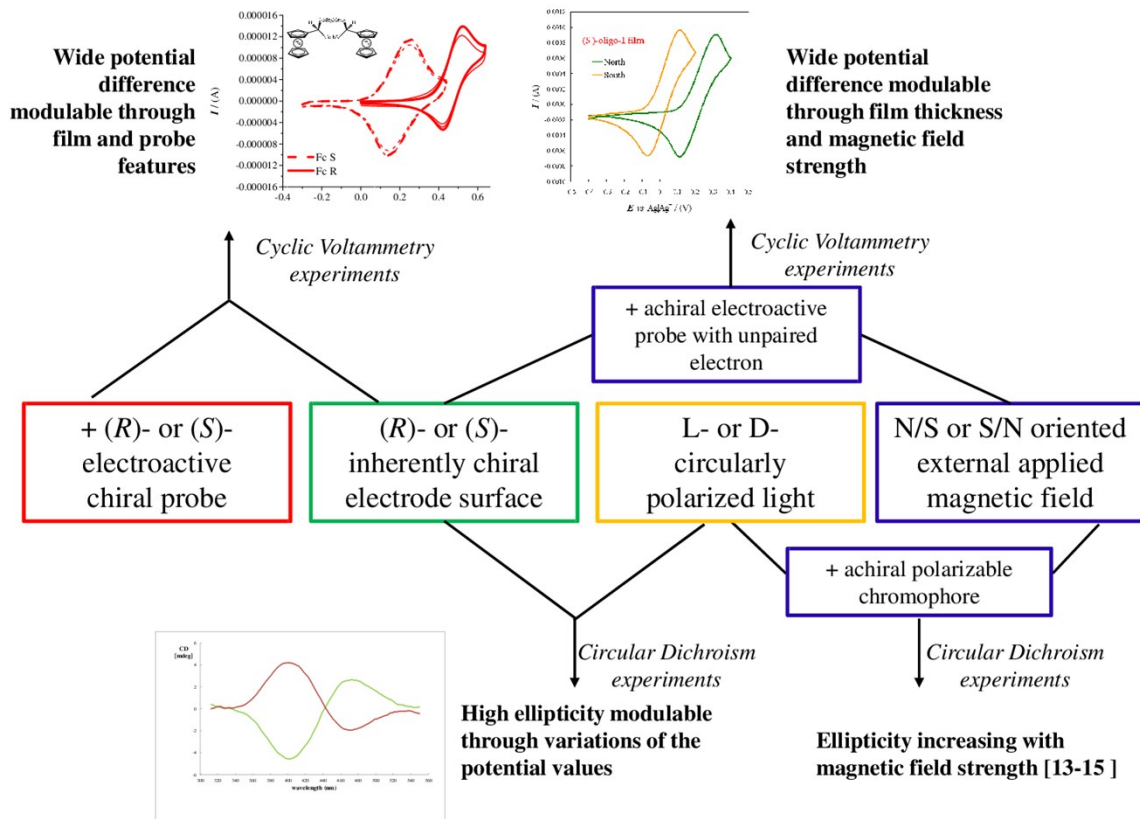**Figure SI.10.3.** ^{1}H NMR (400 MHz, CDCl$_3$) of **(N-Me-IND)$_2$-T$_4$**.

Figure SI.10.4.. ^{13}C NMR (101 MHz, CDCl$_3$) of **(N-Me-IND)$_2$-T$_4$**.

Wide potential difference modulable through film and probe features

Cyclic Voltammetry experiments

Wide potential difference modulable through film thickness and magnetic field strength

Cyclic Voltammetry experiments

+ achiral electroactive probe with unpaired electron

+ (R)- or (S)- electroactive chiral probe

(R)- or (S)- inherently chiral electrode surface

L- or D- circularly polarized light

N/S or S/N oriented external applied magnetic field

+ achiral polarizable chromophore

Circular Dichroism experiments

Circular Dichroism experiments

High ellipticity modulable through variations of the potential values

Ellipticity increasing with magnetic field strength [13-15]

SI. 12 References

1. E. Castiglioni, S. Abbate, G. Longhi. *Appl. Spectrosc.* 2010, **64**, 1416.

2. M. J. Frisch, G. W. Trucks, H. B. Schlegel, G. E. Scuseria, M. A. Robb, J. R. Cheeseman, G. Scalmani, V. Barone, B. Mennucci, G. A. Petersson, *et al.,* GAUSSIAN 09 (Revision A.02), Gaussian Inc., Wallingford CT, **2009**

3. P. J. Stephens. *J. Phys. Chem.* 1985, **89**, 748.

4. F. Furche, R. Ahlrichs, C. Wachsmann, E. Weber, A. Sobanski, F. Vögtle, S. Grimme, *J. Am. Chem. Soc.,* 2000, **122**, 1717.

5. J. Casado, R. Ponce Ortiz, M.C. Ruiz Delgado, R. Azumi, R.T. Oakley, V.Hernández, J.T. López Navarrete. *J. Phys. Chem. B* 2005, **109**, 10115.

6. R. C. González-Cano, G. Saini, J. Jacob, J.T. López Navarrete, J. Casado, M.C. Ruiz Delgado. *Chem. Eur. J.* 2013, **19**, 17165.

7. G. Longhi, S. Abbate, G. Mazzeo, E. Castiglioni, P. Mussini, T. Benincori, R. Martinazzo, F. Sannicolò. *J. Phys. Chem. C* 2014, **118,** 16019.

8. F. Sannicolò, S. Rizzo, T. Benincori, W. Kutner, K. Noworyta, J. W. Sobczak, V. Bonometti, L. Falciola, P. R. Mussini., M. Pierini. *Electrochim. Acta,* 2010, **55**, 8352.

9. R. S. Drago, *Physical Methods in Chemistry*, W.B. Saunders Company Ed., Philadelphia, PA, 1977.

10. T. Benincori, G. Appoloni, P. R. Mussini, S. Arnaboldi, R. Cirilli, E. Quartapelle Procopio, M. Panigati, S. Abbate, G. Mazzeo, G. Longhi, *Chem. Eur. J.* 2018, **284**, 513.

11. J. R. Lacowicz, *Principles of Fluorescence Spectroscopy*, 2nd ed., Kluwer, New York, 1999.

12. F. Sannicolò, S. Arnaboldi, T. Benincori, V. Bonometti, R. Cirilli, L. Dunsch, W. Kutner, G. Longhi, P. R. Mussini., M. Panigati, M. Pierini, S. Rizzo, *Angew. Chem. Int. Ed.*, 2014, **53**, 2623.

13 P.J. Stephens, Ann. Rev. Phys. Chem. 1974, 25, 201.

14 P.J. Stephens, Adv. Chem. Phys. 1976, 35, 197.

15 W.R. Mason, A Practical Guide to Magnetic Circular Dichroism Spectroscopy. Wiley & Sons, Inc. 2007.